

# Plastinated tissue samples as three-dimensional models for optical instrument characterization

Daniel L. Marks, Eric J. Chaney, and Stephen A. Boppart<sup>†</sup>

*Beckman Institute for Advanced Science and Technology, University of Illinois at Urbana-Champaign, 405 N. Mathews Ave., Urbana IL 61801, <sup>†</sup>Also at Departments of Bioengineering, Electrical and Computer Engineering, and Internal Medicine, University of Illinois at Urbana-Champaign.*

[boppart@illinois.edu](mailto:boppart@illinois.edu)

**Abstract:** Histology of biological specimens is largely limited to investigating two-dimensional structure because of the sectioning required to produce optically thin samples for conventional microscopy. With the advent of three-dimensional optical imaging technologies such as optical coherence tomography (OCT), diffuse optical tomography (DOT), and multiphoton microscopy (MPM), methods of tissue preparation that minimally disrupt three-dimensional structure are needed. We propose plastination as a means of transforming tissues into three-dimensional models suitable for optical instrument characterization. Tissues are plastinated by infusing them with transparent polymers, after which they can be safely handled, unlike fresh or fixed tissues. Such models are useful for investigating three-dimensional structure, testing and comparing the performance of optical instruments, and potentially investigating tissue properties not normally observed after the three-dimensional scattering properties of a biological samples are lost. We detail our plastination procedures and show examples of imaging several plastinated tissues from a pre-clinical rat model using optical coherence tomography.

© 2008 Optical Society of America

**OCIS codes:** (180.6900) Three-dimensional microscopy; (000.1430) Biology and medicine; (110.4500) Optical coherence tomography; (120.4800) Optical standards and testing; (170.6935) Tissue characterization

---

## References and links

1. J. G. Fujimoto, M. E. Brezinski, G. J. Tearney, S. A. Boppart, B. E. Bouma, M. R. Hee, J. F. Southern, and E. A. Swanson, "Biomedical imaging and optical biopsy using optical coherence tomography," *Nat. Med.* **1**, 970–972 (1995).
2. A. P. Gibson, J. C. Hebden, and S. R. Arridge, "Recent advances in diffuse optical imaging," *Phys. Med. Biol.* **50**, R1–R43 (2005).
3. W. Denk, J. H. Strickler, and W. W. Webb, "Two-photon laser scanning fluorescence microscopy," *Science* **248**, 73–76 (1990).
4. G. von Hagens, "Impregnation of Soft Biological Specimens with Thermosetting Resins and Elastomers," *Anat. Rec.* **194**, 247–256 (1979).
5. G. von Hagens, K. Tiedemann, and W. Kriz, "The current potential of plastination," *Anat. Embryol.* **175**, 411–421 (1987).
6. H. C. Bickley, A. N. Walker, R. L. Jackson, and R. S. Donner, "Preservation of pathology specimens by silicone plastination. An innovative adjunct to pathology education," *Am. J. Clin. Pathol.* **88**, 220–223 (1987).

7. M. Firbank, M. Oda, and D. T. Delpy, "An improved design for a stable and reproducible phantom material for use in near infrared spectroscopy and imaging," *Phys. Med. Biol.* **40**, 955–961 (1995).
8. D. Passos, J. C. Hebden, P. N. Pinto, and R. Guerra, "Tissue phantom for optical diagnostics based on suspension of microspheres with a fractal size distribution," *J. Biomed. Opt.* **10**, 064,036–1–064,036–11 (2005).
9. J. C. Hebden, B. D. Price, A. P. Gibson, and G. Royle, "A soft deformable tissue-equivalent phantom for diffuse optical tomography," *Phys. Med. Biol.* **51**, 5581–5590 (2006).
10. G. Marquez and L. V. Wang, "White light oblique incidence reflectometer for measuring absorption and reduced scattering spectra for tissue-like turbid media," *Opt. Express* **1**, 454–459 (1997).
11. M. Canpolat and J. R. Mourant, "Particle size analysis of turbid media with a single optical fiber in contact with the medium to deliver and detect white light," *Appl. Opt.* **40**, 3792–3799 (2001).
12. K. W. Gossage, C. M. Smith, E. M. Kanter, L. P. Hariri, A. L. Stone, J. J. Rodriguez, S. K. Williams, and J. K. Barton, "Texture analysis of speckle in optical coherence tomography images of tissue phantoms," *Phys. Med. Biol.* **51**, 1563–1575 (2006).
13. V. Sankaran, J. T. Walsh, Jr., and D. J. Maitland, "Polarized light propagation through tissue phantoms containing densely packed scatterers," *Opt. Lett.* **25**, 239–241 (2000).
14. C.-E. Bisailon, G. Lamouche, R. Maciejko, M. Dufour, and J.-P. Monchalain, "Deformable and durable phantoms with controlled density of scatterers," *Phys. Med. Biol.* **53**, N237–N247 (2008).
15. M. Firbank and D. T. Delpy, "A design for a stable and reproducible phantom for use in near infrared imaging and spectroscopy," *Phys. Med. Biol.* **38**, 847–853 (1993).
16. R. Cubeddu, A. Pifferi, P. Taroni, A. Torricelli, and G. Valentini, "A solid tissue phantom for photon migration studies," *Phys. Med. Biol.* **42**, 1971–1979 (1997).
17. G. Wagnires, S. Cheng, M. Zellweger, N. Utke, D. Braichotte, J.-P. Ballini, and H. Bergh, "An optical phantom with tissue-like properties in the visible for used in PDT and fluorescence spectroscopy," *Phys. Med. Biol.* **42**, 1415–1426 (1997).
18. A. M. De Grand, S. J. Lomnes, D. S. Lee, M. Pietrzykowski, S. Ohnishi, T. G. Morgan, A. Gogbashian, R. G. Laurence, and J. V. Frangoni, "Tissue-Like Phantoms for Near-Infrared Fluorescence Imaging System Assessment and the Training of Surgeons," *J. Biomed. Opt.* **11**, 014,007 (2006).
19. X. Liang, A. L. Oldenburg, V. Crecea, E. J. Chaney, and S. A. Boppart, "Optical micro-scale mapping of dynamic biomechanical tissue properties," *Opt. Express* **16**, 11,052–11,065 (2008).
20. K. Vishwanath, W. Zhong, M. Close, and M.-A. Mycek, "Fluorescence quenching by polystyrene microspheres in UV-visible and NIR tissue-simulating phantoms," *Opt. Express* **14**, 7776–7788 (2006).
21. C. Xu, J. Ye, D. L. Marks, and S. A. Boppart, "Near-infrared dyes as contrast-enhancing agents for spectroscopic optical coherence tomography," *Opt. Lett.* **29**, 1647–1649 (2004).
22. J. Y. Qu, Z. Huang, and J. Hua, "Excitation-and-Collection Geometry Insensitive Fluorescence Imaging of Tissue-Simulating Turbid Media," *Appl. Opt.* **39**, 3344–3356 (2000).
23. B. W. Pogue and M. S. Patterson, "Review of tissue simulating phantoms for optical spectroscopy, imaging and dosimetry," *J. Biomed. Opt.* **11**, 041,102–1–16 (2006).
24. C. H. Fox, F. B. Johnson, J. Whiting, and P. P. Roller, "Formaldehyde Fixation," *J. Histochem. Cytochem.* **33**, 845–853 (1985).
25. J. A. Kiernan, "Formaldehyde, formalin, paraformaldehyde, and glutaraldehyde: what they are what they do," *Microscopy Today* **00-1**, 8–12 (2000).
26. P.-L. Hsiung, P. R. Nambiar, and J. G. Fujimoto, "Effect of tissue preservation on imaging using ultrahigh resolution optical coherence tomography," *J. Biomed. Opt.* **10**, 064,033–1–064,033–6 (2005).
27. C. Pitris, T. Ko, W. Drexler, R. Ghanta, X. Li, C. Chudoba, I. Hartl, and J. G. Fujimoto, "Ultrahigh-resolution *in vivo* versus *ex vivo* OCT imaging and tissue preservation," *Proc. SPIE* **4251**, 170–173 (2001).
28. N. Feder and R. L. Sidman, "Methods and Principles of Fixation by Freeze-Substitution," *J. Biophys. Biochem. Cytol.* **4**, 593–602 (1958).
29. M. T. E. Fahlman, "An Acetone-Vapor Reducing Method for Freeze-Substitution," *J. Int. Soc. Plastination* **12**, 15–16 (1997).
30. T. S. Ralston, D. L. Marks, S. A. Boppart, and P. S. Carney, "Inverse scattering for high-resolution interferometric microscopy," *Opt. Lett.* **31**, 3585–3587 (2006).
31. T. S. Ralston, D. L. Marks, P. S. Carney, and S. A. Boppart, "Inverse scattering for optical coherence tomography," *J. Opt. Soc. Am. A* **23**, 1027–1037 (2006).
32. T. S. Ralston, D. L. Marks, P. S. Carney, and S. A. Boppart, "Interferometric synthetic aperture microscopy," *Nat. Phys.* **5**, 129–134 (2007).
33. U. Morgner, W. Drexler, F. X. Kartner, X. D. Li, C. Pitris, E. P. Ippen, and J. G. Fujimoto, "Spectroscopic optical coherence tomography," *Opt. Lett.* **25**, 111–113 (2000).
34. M. A. Choma, M. V. Sarunic, Y. Changhuei, and J. A. Izatt, "Sensitivity advantage of swept source and Fourier domain optical coherence tomography," *Opt. Express* **11**, 2183–2189 (2003).
35. A. M. Zysk, E. J. Chaney, and S. A. Boppart, "Refractive index of carcinogen-induced rat mammary tumours," *Phys. Med. Biol.* **51**, 2165–2177 (2006).
36. D. L. Marks, S. C. Schlachter, A. M. Zysk, and S. A. Boppart, "Group refractive index reconstruction with

## 1. Introduction

Histology is an indispensable tool for understanding the microscopic anatomy and pathology of biological tissues. The diversity of fixation, sectioning, and staining methods used in histological preparation make it a tool of biomedical research of unmatched versatility, representing the “gold standard” for pathology. Unfortunately, because of the need to section the tissue, histology inherently disrupts the three-dimensional structure and so is used largely to study two-dimensional features. Non-invasive and minimally invasive imaging methods such as optical coherence tomography [1], diffuse optical tomography [2], and multiphoton microscopy [3] are able to image three-dimensional structure *in vivo*. Such methods have created a need for three-dimensional optical phantoms for testing, and tissue preparation methods that disrupt three-dimensional structure less than sectioning. In this work, we propose plastination [4, 5, 6] as a tissue preparation method that better preserves three-dimensional structure for study by these new optical imaging techniques. The method arrests decay in the sample, and embeds it in highly transparent silicone or epoxy to create a high-quality optical interface into the tissue. After embedding, the sample is odorless and can be handled without gloves. The method presented here is suitable for small samples and is simplified to use readily available chemicals and equipment rather than a dedicated plastination facility. In this article, we detail the plastination procedures for embedding tissues in both epoxy and silicone polymers and show examples of plastinated tissue from a pre-clinical rat model imaged with optical coherence tomography.

Plastination, invented by Gunther von Hagens, is a method of preserving tissue by replacing water and lipids with cured polymers [4, 5, 6]. The preserved tissues can last indefinitely and retain most microscopic features. After the polymer is cured, the samples are durable, can be handled safely, and are useful for anatomical instruction. Infusion of cured epoxy polymers into tissues is also used in electron ultrastructure microscopy to preserve nm-scale details, which suggests that polymer embedding might also be useful for microscopy studies of tissue microstructure. For these reasons we investigated plastination as a means of transforming tissues into plastinated models.

Due to the specialized equipment and chemicals frequently needed for plastination, we desired to simplify the process and embed the sample completely in polymer. Samples imaged for OCT are typically less than one centimeter in size, for which the embedding process can be completed in less than a month. Furthermore, samples of this size are easy and inexpensive to embed completely in polymers, so that the cured polymer protects and supports the sample and forms an optical interface to the irregular sample surface as an index matching medium.

Others have taken a different approach to tissue models, which are typically tissue phantoms constructed of artificial materials. Phantoms often include microspheres of silica or polystyrene embedded in polymer [7, 8, 9, 10, 11, 12, 13, 14] because the refractive indices and dimensions of these materials are known precisely and Mie scattering theory can be used to predict the scattering coefficient, phase function, and absorption of these phantoms. Intralipid, titanium dioxide particles, agar, and gelatin [15, 16, 17, 18, 19] are also used to create turbid media with scattering properties similar to tissues. Dyes [17, 18, 20, 21, 22] are added as contrast agents for fluorescence imaging or as background absorbers to approximate the absorption properties of tissue. A detailed survey of tissue phantom construction methods is conducted by Pogue and Patterson [23]. These phantoms are generally designed to be simple, predictable, reproducible, and to have optical scattering and absorption properties quantitatively similar to real tissues. Because of their simplicity, phantoms necessarily only incorporate those properties of tissues that the designers believe are relevant. Even though the plastinated specimens are not engineered from standardized materials like artificial phantoms, plastinated specimens

are likely to retain scattering features that would not be deliberately designed into an artificial phantom. Plastinated specimens offer a new way to characterize imaging systems that does not require fresh or fixed tissue, but is more like fresh tissues than artificial phantoms.

In order to explore how to plastinate tissue as optical models, we plastinated formalin-fixed pre-clinical rat model tissues. We embedded tissues in two different polymer types: epoxy and polydimethylsiloxane (silicone). These are the two most common types of polymer used for plastination. Silicone plastination is typically used to preserve anatomical specimens for public display and anatomical instruction. Samples that are plastinated using BIODUR S10 by BIODUR Products (Heidelberg, Germany) tend to have a rubbery texture and opaque appearance similar to human flesh. For our purposes, the turbidity introduced by the BIODUR S10 made it unsuitable for optical coherence tomography, but turbidity may be an advantage for DOT. Epoxy plastination, such as with BIODUR E12/E6 polymer, tends to produce highly transparent and rigid specimens. The transparency introduced by epoxy impregnation is an advantage for microscopic analysis, and the rigidity can help stabilize the microstructure as it does in epoxy-impregnated samples for electron ultrastructure microscopy. Other polymer types can be used such as polyester or polyurethane [4], which can produce different degrees of turbidity and scattering contrast with embedding tissue.

There are four main steps to the plastination process: fixation, dehydration, impregnation, and polymerization. Fixation, which is typically achieved with formalin [24], strengthens weak structure and deactivates enzymes by crosslinking proteins [25] that otherwise would cause autolytic decomposition of the tissue. Fixation is necessary because otherwise enzymes in the tissue continue decomposition over long periods of time even after dehydration. The effects of fixation and other tissue preservation methods on the scattering properties of tissues were investigated [26, 27] using OCT. Dehydration replaces the water in the tissue with a volatile solvent that is miscible with both water and the monomer that will be infused into the tissue. The dehydration can occur in stages with the water and other solvents being progressively replaced (e.g. immersion in increasing concentrations of ethanol, acetone, or methylene chloride) while in the liquid state. Another possibility is to use freeze substitution [28], where the tissue is quickly frozen to stabilize structure, and the immersing dehydration solvent (which is liquid below 0 deg C) slowly dissolves and replaces the ice in the tissue. To impregnate the sample with monomer, the sample is placed into a bath of monomer so that the monomer will diffuse into the tissue. Vacuum infiltration is often used to remove the volatile solvent by placing the sample into a vacuum chamber, so that monomer will be drawn into the tissue as the solvent evaporates. Finally, the monomer is allowed to polymerize, so that the plastic can support and stabilize the structure of the tissue. After polymerization, the tissue is solid and can usually be handled without special precautions unlike fixed or biohazardous tissue.

## 2. Materials and methods

Below we describe both silicone and epoxy methods of plastination. The equipment needed for both methods consists of a refrigerator at 5-10 deg C, a freezer at -25 to -15 deg C, and a vacuum chamber at room temperature (20 to 25 deg C). Supplies that will be needed include sealable vials that can contain acetone (avoid polystyrene containers), sealable polyethylene bags [29] to prevent vapors from escaping inside the freezer, 35 mm diameter polystyrene dishes to contain the final specimen, and 22 mm square microscope cover slips. Pure acetone is used in both processes as the dehydrating solvent, and formalin is used as the fixing agent.

The silicone embedding process does not use the common BIODUR S10 polymer. Our goal was to minimize the scattering of the sample, and the product of S10 plastination is turbid. Instead, we devised our own plastination process based on commonly available silicone oil (50 cSt, Clearco Inc., Bensalem, PA), and Sylgard 184 polydimethylsiloxane (PDMS) elas-

tomers and hardeners (Dow Corning, Inc., Midland, MI). The elastomer is commonly used for microfluidic devices, and is quite transparent. The sample is impregnated with silicone oil, and the elastomer/hardener forms a protective, index-matching silicone medium which supports the sample. The steps of the silicone process are as follows:

1. Fix the sample in a 2% formalin solution at 5-10 deg C for 7 days.
2. For each sample, prepare two vials: one filled with acetone and another with silicone oil. The volume of the vials should be at least twenty times that of the sample itself. Completely seal the vials and place them into sealed polyethylene bags to prevent flammable acetone vapors from escaping. Place the vials into the freezer and allow them to cool to freezer temperature.
3. Place the tissue into the cold acetone vial, seal the vial in a polyethylene bag, and then place the bag in the freezer. Inside the sample, the water is replaced by acetone by freeze substitution. Keep the sample in the acetone vial for seven days or more to thoroughly dehydrate the sample.
4. Remove the samples from the acetone vials and immediately transfer the samples into the silicone oil vial. Immediately close the vial and tumble the vial to completely cover the sample in silicone oil. Seal the vial in a polyethylene bag, and place the bag in the freezer for at least 72 hours. The silicone oil will replace the acetone inside the sample at freezer temperatures, also minimizing shrinkage.
5. To complete the substitution of acetone with silicone oil by vacuum infiltration, remove the silicone oil vial from the freezer and place the opened vial in the vacuum chamber at room temperature for 72 hours.
6. Remove the samples from the silicone oil and allow the excess silicone oil to drip off.
7. Prepare the PDMS by mixing 10 parts of Sylgard 184 elastomer to 1 part hardener. Place this mixture into the vacuum chamber for 30 minutes to remove air bubbles. Pour a thin layer of the PDMS at the bottom of a specimen dish and place the sample at the bottom of the dish. Allow the PDMS to cure for 24 hours at room temperature, adhering the sample at the bottom of the dish, preventing the sample from floating in the PDMS.
8. Prepare PDMS as described above. Pour the PDMS into the dish until the sample is barely submerged (0.5 to 1.0 mm depth). Be careful to pour slowly and continuously as to not introduce any air bubbles into the PDMS. Allow the PDMS to fully cure for at least 24 hours at room temperature.
9. Finally, adhere a microscope coverslip on top of the sample. A coverslip adhered to the surface is a clear, durable, and cleanable optical window into the medium. Prepare PDMS as described above. Using a thin wooden applicator (toothpick), carefully place a droplet of PDMS onto the tip of the toothpick without introducing any air bubbles into the PDMS. Do this by dipping the end of the toothpick into the uncured PDMS and rolling the toothpick between one's fingers to grow the droplet. When the droplet is large enough (4 to 7 mm in diameter), drip it onto the surface of the PDMS inside the dish. Place another PDMS droplet on the toothpick and drip it onto the center of a coverslip. Allow both droplets to spread out slightly over a minute or two. Then invert the coverslip and place its droplet in contact with the droplet inside the dish. Do not push downward; allow the weight of the droplet and the coverslip to spread the PDMS over the surface of the sample. Allow 24 hours for the PDMS to cure.

The plastination procedure with epoxy samples uses the BIODUR E6/E12/E600 process, with E12 being the resin, E6 the hardener, and E600 the accelerator. Unlike the silicone process, in which the silicone oil is not crosslinked inside the specimen, the epoxy will be crosslinked throughout the specimen, lending increased structural rigidity. This requires modification of the procedure, which is detailed below:

1. Fix the sample in a 2% formalin solution at 5-10 deg C for 7 days.
2. Chill sealed vials of acetone at freezer temperature (-25 to -15 deg C). The volume of the acetone should be at least 20 times that of the sample in each vial.
3. Transfer samples directly from the formalin to the chilled acetone vials so that the samples immediately freeze and freeze substitution occurs. Completely seal the vials and place them into sealed polyethylene bags to prevent flammable acetone vapors from escaping. Allow the samples to dehydrate in the acetone for 7 days.
4. Prepare the epoxy by combining 50 g BIODUR E12 resin, 25 g BIODUR E6 hardener, and 1 mL BIODUR E600 accelerator. Place the mixture into vials and chill to freezer temperature.
5. Transfer the samples directly from the acetone to the epoxy vials quickly. Tumble the sealed vials to ensure the sample is completely covered by the epoxy. If the acetone is allowed to evaporate from the surface, a dry spot may occur into which the epoxy poorly penetrates. Seal the vials in a polyethylene bag, and then place the bag in the freezer for 2 days. The cold temperature will slow the polymerization of the epoxy.
6. Remove the vials from the freezer. Place the samples into polystyrene petri dishes, pouring a small amount of epoxy into the bottom of the dish to ensure there are no air bubbles between the sample and the dish bottom. Place the petri dishes into a vacuum chamber at room temperature (25 C) for five days, during which vacuum infiltration of the epoxy occurs and the epoxy hardens.
7. After the samples have hardened, mix more epoxy using the ratios as stated above. Place this mix into the vacuum chamber for an hour to allow the air to bubble out. Pour the mixed epoxy into the petri dishes until the samples are slightly submerged in epoxy. Pour slowly and from a low height to avoid introducing more air bubbles into the epoxy. Allow the samples to cure at room temperature in air for 7 days.
8. After the submerging epoxy has hardened, mix more epoxy (from 5 to 10 g) using the ratios as stated above. Place this mix into the vacuum chamber to remove air bubbles. Place a drop of the epoxy (approximately 0.1 mL) on the hardened epoxy surface above the sample in each petri dish. Take a coverslip and place it on the droplet as to allow the air to be pushed out from under the coverslip by the weight of the coverslip. Avoid pushing down on the coverslip. By leaning the coverslip on one side of the droplet, the air is pushed to the other side of the droplet so that air is not trapped beneath the coverslip. Allow the samples to cure for 7 days at room temperature in air.

While adhering coverslips to the surface of the samples is not required, it is highly recommended. The coverslips will provide a more uniform optical interface into the polymer than the exposed polymer itself. The exposed epoxy surface has a tendency to crystallize and become cloudy without a coverslip holding its shape. The coverslips will also be much easier to keep clean and will better resist abrasion than plastic. The coverslip surface can be used to deflect specular reflections of the incident beam when imaging with OCT. A cover slip can also be used

as a reference delay surface rigidly coupled to the sample, which is useful for phase-resolved methods such as spectroscopic OCT [30, 31, 32] and Interferometric Synthetic Aperture Microscopy [33, 21].

### 3. Results and discussion

To demonstrate this process, organs were harvested from rats and plastinated. The animals used in this study were cared for and handled under a protocol approved by the Institutional Animal Care and Use Committee of the University of Illinois at Urbana-Champaign. The tissues preserved included lung, cardiac muscle, skeletal muscle, cornea, and adipose tissue. The animal was euthanized by carbon dioxide asphyxiation and the organs were immediately dissected. The dissected organs were placed into the 2% formalin and into refrigeration as detailed above to begin the embedding process.

After the embedding, the samples were volumetrically imaged in three-dimensions using OCT. The OCT instrument used to image the samples used spectral-domain detection [34], with an axial resolution of  $3\ \mu\text{m}$  and transverse resolution of  $8\ \mu\text{m}$  sensing in the 800 nm band. The incident power on the sample was 10 mW. The dimensions of the acquired data volumes were approximately 1800 by 1000 by 1300  $\mu\text{m}$  in depth. Over the long axis and depth (1800x1300  $\mu\text{m}$ ), two-dimensional Interferometric Synthetic Aperture Microscopy [31, 32] algorithms were used to correct for defocus. Because the cover slip reflection could not be isolated in each OCT interferogram, a consistent phase reference for all axial scans of a given three-dimensional volume was not available. Therefore phase stability problems due to vibration and long-term phase drift could not be compensated for and ISAM defocus correction was only achieved in the fast transverse scan direction.

As a first demonstration, Fig. 1 shows the results of silicone plastination of skeletal muscle. Part (a) is a B-mode section and (b) an *en face* section of the muscle. The relative orientations of the sections are shown in (c) as a three-dimensional rendering with the corresponding axes labeled. The data were processed into DICOM format using ImageJ (<http://rsbweb.nih.gov/ij/>) and digitally sectioned and rendered using 3D Slicer (<http://www.slicer.org/>). In the B-mode section, the fasciculi are clearly visible separated by perimysia. This results in the striated skeletal muscle image. The contrast is opposite of a conventional hematoxylin and eosin stained skeletal muscle section, as the perimysia scatter more in the plastinated sample, whereas the fasciculi are stained more by H&E. It may be possible to reimpregnate a silicone-impregnated sample with paraffin if histological sectioning is desired because the silicone oil might be removed with solvents, but this was not attempted. Part (d) is a photograph of the preserved skeletal muscle sample. The photograph shows a textured epimysium which was smooth before the silicone impregnation step. The muscle was also somewhat larger before the impregnation. When the sample is not formalin fixed before silicone embedding, the shrinking is reduced, but unfortunately the sample degrades over time due to autolytic decomposition. A lower viscosity silicone oil would probably diffuse into the tissue more easily and reduce shrinkage.

For comparison, Fig. 2 shows the OCT image sections of an epoxy plastinated skeletal muscle. Again, part (a) is a B-mode section, and (b) an *en face* section, with (c) showing their relative orientation. The epoxy plastination process produces less shrinkage than the silicone plastination. This is likely due to the ease of diffusion of the smaller epoxy monomer molecules compared to the large polydimethylsiloxane oil molecules during impregnation. The fasciculi and perimysia can be seen in cross-section in the *en face* image clearly. The imaging penetration is also improved over the silicone embedded sample due to the reduced scattering of the sample. The weaker scattering also affected the axial scan integration time, because more weakly scattering samples return less power and therefore require a longer integration time to

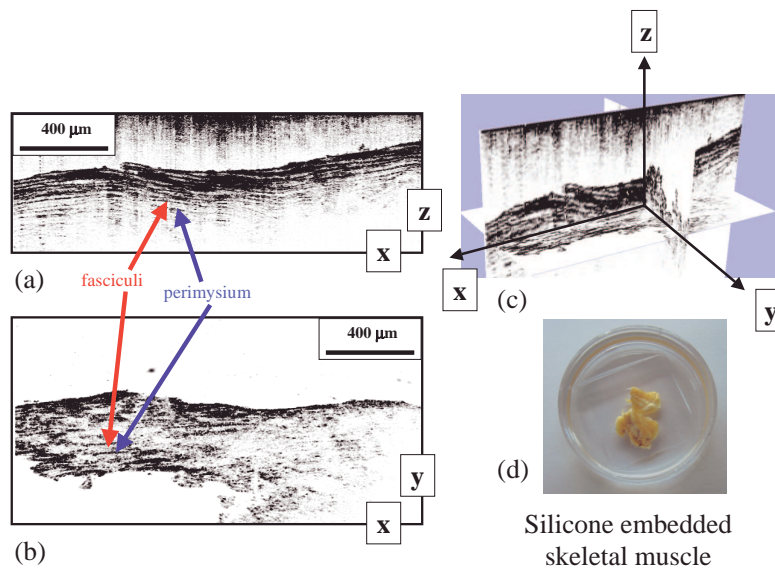


Fig. 1. OCT image sections from a 3-D OCT data set of a silicone plastinated skeletal muscle. Part (a) is a B-mode section, and (b) is an *en face* section. Part (c) is a rendering of the relative orientations of the sections with the axes marked corresponding to the section axes. Part (d) is a photograph of the plastinated sample.

achieve a particular signal-to-noise ratio. Because of the reduced scattering, the epoxy samples required an exposure time of 10 ms per axial scan, as compared to a 200  $\mu$ s to 1 ms per scan for silicone samples.

Figure 3 contains images from a 3-D OCT data set of epoxy plastinated cardiac muscle. At this scale, cardiac and skeletal muscle look similar because cardiac-specific features such as intercalated discs are too small to resolve. The contrast here is opposite to that of the silicone or epoxy embedded muscle, and more like standard H&E stain. Comparing the color of the cardiac muscle and the skeletal muscle in the included photographs, the cardiac muscle is clearly darker and redder, which may be due to blood remaining in the heart muscle. The blood could also produce additional scattering throughout the bulk of the muscle compared to the skeletal muscle. The depth penetration in the image of the cardiac muscle is slightly better than epoxy-plastinated skeletal muscle image. In the image, the apparent attenuation is determined both by scattering and by the finite depth-of-focus of the imaging system (approximately 500  $\mu$ m), so that in this case the depth-dependent signal may be determined more by the depth-of-field of the lens than the sample scattering.

The reduced scattering in the epoxy plastinated specimens may be explained by the higher refractive index of Biodur E6/E12 epoxy at 1.551, compared to silicone oil with an index of 1.402, excised stroma with an index of 1.388, and adipose tissue with an index of 1.467 [35]. The refractive index of tissues is an average over the constituents including the water and lipids which make up the bulk. The lower scattering of the epoxy samples suggests that the refractive index of the remaining constituents after replacement of the water and lipids may be more like that of epoxy than silicone, because the backwards scattering contrast is due to the difference between the bulk refractive index and the wavelength-scale features that produce backscattering. Using a novel confocal microscope design [36], future work will directly measure the

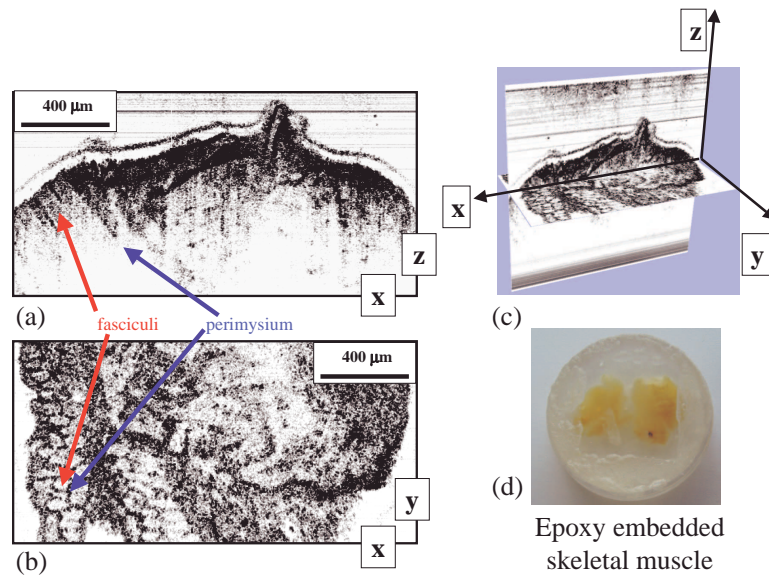


Fig. 2. OCT image sections from a 3-D OCT data set of an epoxy plastinated skeletal muscle. Part (a) is a B-mode section, and (b) is an *en face* section. Part (c) is a rendering of the relative orientations of the sections with the axes marked corresponding to the section axes. Part (d) is a photograph of the plastinated sample.

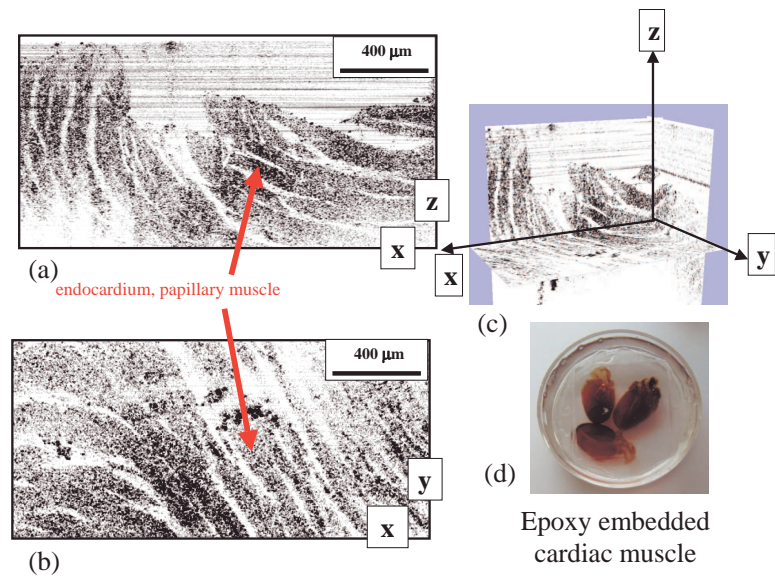


Fig. 3. OCT image sections from a 3-D OCT data set of an epoxy plastinated cardiac muscle. Part (a) is a B-mode section, and (b) is an *en face* section. Part (c) is a rendering of the relative orientations of the sections with the axes marked corresponding to the section axes. Part (d) is a photograph of the plastinated sample.

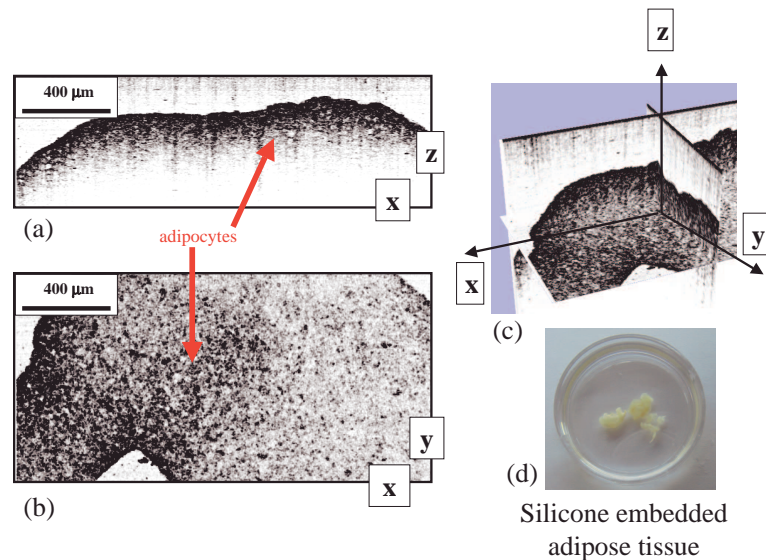


Fig. 4. OCT image sections from a 3-D OCT data set of silicone plastinated adipose tissue. Part (a) is a B-mode section, and (b) is an *en face* section. Part (c) is a rendering of the relative orientations of the sections with the axes marked corresponding to the section axes. Part (d) is a photograph of the plastinated sample.

refractive index of these wavelength-sized features while minimally altering the tissue. Regardless of its origin, the decreased scattering of epoxy plastinated samples is an opportunity to image deeper structure and larger volumes than would otherwise be accessible.

Another example comparing the silicone and epoxy processes is shown in Figs. 4 and 5, in which adipose tissue was plastinated. In both examples, the cellular structure of the adipocytes is visible. The dark areas at the top of the volume are the autocorrelation image, and is an artifact of spectral-domain OCT imaging. The shrinkage was much greater with the silicone sample of Fig. 4 than the epoxy sample, which is also visible in the photograph. The scattering of the epoxy sample is far less, with the exposure time being ten times as long for the epoxy sample (10 ms per scan, vs. 1 ms for the silicone). Therefore a similar trend holds for adipose tissue as well as muscle tissue, with epoxy plastination producing less shrinkage and scattering. The shrinkage in the silicone samples occurs during the silicone oil infiltration step, whereas this shrinkage does not appear during the epoxy infiltration.

Further examples of silicone plastination are shown in Figs. 6 and 7. Figure 6 is of a plastinated cornea. The layers of the cornea remain distinct even after plastination. The transparency of the cornea is largely preserved after silicone impregnation. The plastinated lung tissue in Fig. 7 shows bronchioli below the surface in the *en face* image of part (b), with an oblique slice taken to correspond to features below but parallel to the surface of the lung. Because the air and fluids in the lung have been replaced by silicone oil throughout, the scattering is reduced and it is easier to see the interior airways of the lung.

In summary, we have demonstrated plastination as a means to create tissue models using harvested tissues for 3-D optical imaging techniques. After embedding in polymer, the samples are dry and can be handled safely. Our silicone plastination process yields a sample with scattering more like untreated tissue, but suffers from shrinkage artifacts. Histological preparation

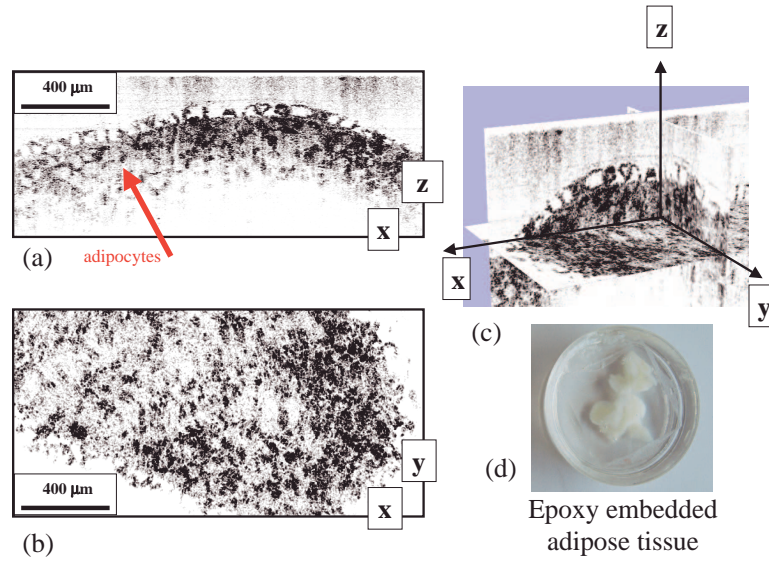


Fig. 5. OCT image sections from a 3-D OCT data set of epoxy plastinated adipose tissue. Part (a) is a B-mode section, and (b) is an *en face* section. Part (c) is a rendering of the relative orientations of the sections with the axes marked corresponding to the section axes. Part (d) is a photograph of the plastinated sample.

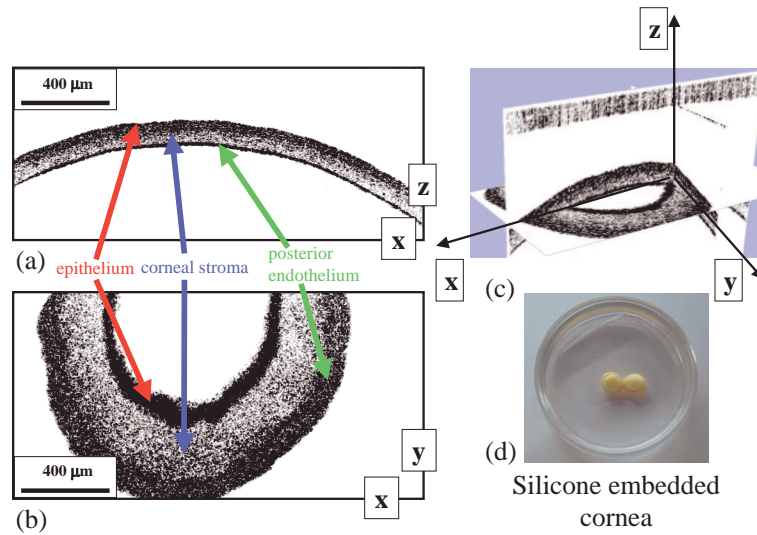


Fig. 6. OCT image sections from a 3-D OCT data set of a silicone plastinated cornea. Part (a) is a B-mode section, and (b) is an *en face* section. Part (c) is a rendering of the relative orientations of the sections with the axes marked corresponding to the section axes. Part (d) is a photograph of the plastinated sample.

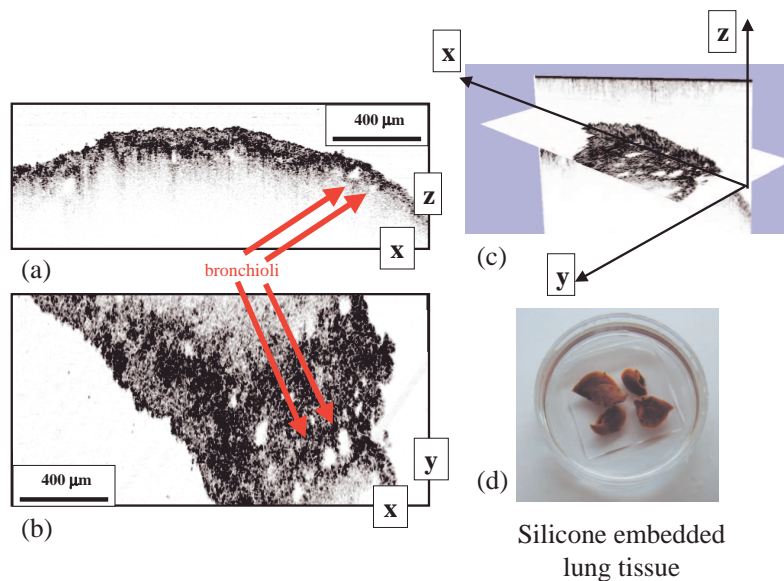


Fig. 7. OCT image sections from a 3-D OCT data set of silicone plastinated lung tissue. Part (a) is a B-mode section, and (b) is an *en face* section. Part (c) is a rendering of the relative orientations of the sections with the axes marked corresponding to the section axes. Part (d) is a photograph of the plastinated sample.

also causes shrinkage artifacts as well as disrupts the 3-D structure, so distortions caused by silicone plastination may still be acceptable in comparison. Reducing the degree of formalin fixation, or using a different fixative to prevent autolytic decomposition of the tissues may reduce this shrinkage. Progressively infusing the tissue with increasingly viscous silicone oils would also likely reduce shrinkage. Epoxy plastination produces highly transparent samples that may be useful to better study deeper structure without sectioning. Future studies will investigate changes in the optical scattering and absorption following plastination, and how these alter the qualitative image features observed with OCT. *En face* optical coherence microscopy will also be used to investigate fresh and plastinated samples to achieve a resolution comparable with histological sectioning, and to examine microstructural changes due to the plastination process. Plastinating specimens is an alternative to histological processing that is better suited to three-dimensional optical imaging techniques and which may offer a practical compromise solution between imaging fixed or live tissues and histological sections.

This work was supported in part by the NIH (1 R01 EB005221, 1 R21 EB005321, 1 R21 CA115536 S.A.B.) and the NSF (BE5 05-19920, BES 03-47747, S.A.B.). More information is available at <http://biophotonics.uiuc.edu>.